Taylor & Francis
Taylor & Francis Group
STLE
Society of Tribologists and Lubrication Engineers
Tribology Transactions

An investigation of lubricant film thickness in sliding compliant contacts

Journal:	*Tribology Transactions*
Manuscript ID:	UTRB-0457.R1
Manuscript Type:	Manuscript for Publication Only
Date Submitted by the Author:	
Complete List of Authors:	Myant, Connor; Imperial College London, Tribology Fowell, Mark; Imperial College London, Department of Mechanical Engineering Spikes, Hugh; Imperial College London, Mechanical Engineering Stokes, Jason; Unilever Corporate Research, Unilever R&D Colworth; University of Queensland, Division of Chemical Engineering
Keywords:	Compliant Surface EHL < EHL, EHL Film Geometry < EHL, Low Elastic Modulus EHL < EHL

An investigation of lubricant film thickness in sliding compliant contacts

Connor Myant[1*], Mark Fowell[1], Hugh A. Spikes[1], Jason R. Stokes[2+].

[1] *Tribology Section*

Department of Mechanical Engineering

Imperial College of Science, Technology and Medicine

London

SW7 2AZ

U.K.

[2] *Unilever Corporate Research*

Unilever R&D Colworth

Colworth House

Sharnbrook

MK44 1LQ

U.K.

[+]*Current Address:*

A/Prof. J.R. Stokes,

Division of Chemical Engineering,

School of Engineering,

University of Queensland,

BRISBANE 4072,

Australia

*Corresponding Author: connor.myant@imperial.ac.uk

Abstract

An optical interferometric technique has been used to investigate fluid film thickness in sliding, isoviscous elastohydrodynamic contacts (I-EHL). Monochromatic 'two-beam' interferometry has been employed to map lubricant film thickness across a range of applied loads and entrainment speeds. The contact was formed between an elastomer sphere and plain glass disc, illuminated under red light, $\lambda = 630$ nm. Experimental work has employed sunflower oil and glycerol/water solutions as the test lubricants, due to their similar refractive indices and varying viscosity. A black and white image intensified camera has been employed to capture interference images and a computer processing technique used to analyse these images, pixel by pixel, and create film thickness maps based on their grey scale intensity representations. Comparison of film thickness results to theoretical models show reasonable qualitative agreement. Experimental results show both a reduced horseshoe, which is limited to the rear of the contact, and 'wedge' shaped film thickness profile within the Hertzian contact region. This is unlike conventional 'hard' EHL contacts where the horseshoe shaped pressure constriction extends around the contact towards the inlet. Experimental results suggest film thickness profiles take on a 'convergent wedge' shape similar to that used in many hydrodynamic bearings. It is likely that this 'wedge' is largely responsible for generating fluid pressure and therefore the load-carrying capacity of the contact.

Keywords: Low Elastic Modulus EHL, Optical Interferometry, Isoviscous-Elastic, Elastohydrodynamic, Elastomeric.

Introduction

The measurement of lubricant film thickness values within a compliant contact is a challenging problem for several reasons (1):

- Lubricant film thickness covers a wide range of values; the required measuring range can be from fractions to the hundreds of microns.
- Contact sizes are considerably larger than those of non-compliant tribological contacts.
- Elastomeric and tissue materials present in most compliant contacts are poor electrical conductors and light reflectors.
- Coating compliant surfaces with reflective layers is difficult as these layers tend to be prone to wear or to influence the compliance and surface properties significantly.
- Many compliant components have a high roughness compared to stiff surfaces and it is very difficult to polish compliant surfaces.

When designing components for use in lubricated, compliant, contacts, the liquid film thickness is a significant parameter in determining friction and wear performance. There exist in the literature a number of regression equations for calculating film thickness (2) derived from numerical simulations, but few experimental techniques for checking the validity of these equations. It is therefore important that solutions are found to the issues listed above. The current paper describes a technique for measuring lubricant film thickness between highly deformable surfaces under low-load/low-pressure conditions using optical interferometry.

Isoviscous-elastic or 'soft-elastohydrodynamic' lubrication (I-EHL) occurs in lubricated contacts between non-conforming bodies when the contact pressure is great enough to cause elastic deformation of one or both of the interacting solids but the pressure within the contact is low and insufficient to cause any substantial change in fluid viscosity (3). The lubricant thickness is therefore independent on the lubricant's pressure-viscosity characteristics but much more strongly dependent on the elastic properties of the contacting surfaces than for conventional EHL. There are a number of regression equations for predicting lubricant film thickness in the I-EHL regime for both line and elliptical contacts. Perhaps the best known of these are the Hamrock and Dowson equations for film thickness in elliptical contacts (4);

$$H_c = 7.32(1-0.72e^{-0.28k})U^{0.64}W^{-0.22} \quad [1]$$

$$H_m = 7.43(1-0.85e^{-0.31k})U^{0.65}W^{-0.21} \quad [2]$$

where H_c and H_m are the dimensionless central and minimum film thicknesses respectively, defined by *h/R'*. *k* is the ellipticity parameter, which reduces to 1 for the circular contact of interest in the current study. Therefore;

$$h_c = 3.3U^{0.64}W^{-0.22}R' \quad [3]$$

$$h_m = 2.8U^{0.65}W^{-0.21}R' \quad [4]$$

where h_c and h_m are the central and minimum film thickness respectively and the dimensionless operating parameters are:

Dimensionless speed parameter, $U = \frac{u\eta}{E'R'}$ [5]

Dimensionless load parameter, $W = \frac{Q}{E'R'^2}$ [6]

where u is the entrainment speed, Q the applied load, η the lubricant dynamic viscosity, R' the reduced radius of curvature in the entrainment direction, and E' the effective elastic modulus. The latter two terms are defined by $1/R' = 1/r_{x1} + 1/r_{x2}$ and $2/E' = (1 - \upsilon_1^2)/E_1 + (1 - \upsilon_2^2)/E_2$, respectively, where r_{x1}, r_{x2}, E_1, E_2, υ_1, and υ_2 denote the radii in the entrainment direction, the Young's moduli, and the Poisson's ratios of the two contacting bodies.

In the current study, a lubricated, compliant contact was produced between a glass flat and an elastomer sphere. This contact was illuminated with a monochromatic light, and an interference image of the contact was detected through the glass using an image-intensified camera. A Rolera MGi B/W camera and electronmultiplier (QImaging, UK) were employed to capture interference images and a computer processing technique was used to analyse these images, pixel by pixel, and create film thickness maps based on their grey scale intensity representations. Tests were carried out over a range of entrainment speeds and applied loads. Results are reported for pure sliding conditions between a rotating polydimethylsiloxane (PDMS) sphere and an uncoated glass flat, lubricated with sunflower oil and glycerol/water solutions.

Contact profile shapes and film thickness maps are compared to theoretical models and discussed.

Background

Currently there exists no straightforward technique for measuring lubricant film thickness within a lubricated, compliant tribological contact. Optical interferometry (5-8), magnetic resistance (1), laser-induced fluorescence (9) and Raman spectroscopy (10) have all been successfully used to measure lubricant film thickness. However, each one of these has limitations and difficulties. As yet there is no established technique for routinely obtaining film thickness data within compliant contact as formed by elastomeric and most biological materials. This is unlike stiff contacts formed by most ceramics and metals, where optical interferometry is now routinely used to measure the EHL film thickness properties of lubricants, while electrical capacitance measurements are often employed to measure EHL and hydrodynamic film thicknesses in engineering components

In an attempt to measure film thicknesses up to the hundreds of microns within compliant contacts, Poll *et al* (1) used an approach involving magnetic flux measurement. Here, magnetite particles were dispersed within the lubricant, using surfactant molecules to protect them against oxidation and coagulation. The particle size (average diameter of 10 nm and maximum of 80 nm) was claimed to be sufficiently small to avoid them having any effect on film formation or wear. A magnetic circuit was built such that magnetic flux was directed through the seal contact. Due to the high permeability of magnetite, the inductivity and impedance of

the coil providing the magnetic potential could be calibrated to indicate the amount of fluid present. Using this method, film thickness was successfully measured within a rotary lip seal. The advantage with this technique is that no optical window is required and the input and output signals are transmitted by the same device (no separate optics for incoming and out outgoing light). The test specimen can also be used with its original surface micro-geometry (no optical transparency is required), allowing rough surfaces to be investigated. This technique suffers from a number of disadvantages. Firstly a magnetic fluid is required and this clearly limits the range of lubricants which can be tested and puts a lower limit on the measurable thickness. Contact profiles of the lubricant film cannot be recorded simultaneously, but only by axial displacement of the sample or test rig (in relation to each other), making film thickness maps difficult to obtain.

Fluorescence microscopy has been successfully applied to study the lubricant film present in complaint contacts (9). A low concentration of fluorescent dye is dissolved in the lubricant which is entrained into the contact. The contact is then illuminated with laser light and a fluorescent image of the contact is produced. Fluorescence intensity is proportional to film thickness, so fluorescent intensity images obtained in this way can be converted into maps of film thickness using a calibration. A further advantage of this technique is the wide range of surface roughness and film thicknesses that can be measured. Limited research has been done using this technique, so the full range of film thickness values obtainable is not yet known. The method requires one of the contacting surfaces to be transparent to visible light, and the technique is also affected by signal noise from the imaging systems employed and from irregularities from the laser, *i.e*. speckle.

Bongaerts *et al* (10) successfully demonstrated the use of confocal Raman spectroscopy to measure lubricant film thickness and composition within a complaint, tribological contact, lubricated with both simple Newtonian fluids and stabilized oil/water emulsions. The system has the added ability of detecting lubricant composition at different positions and depths in the contact. Raman is well suited to study emulsions and semi-opaque lubricants, *e.g.* shampoos. However it has certain limitations. Water has a poor Raman signal, so aqueous solutions need another bulk solvent added to the polar phase, making low viscosity aqueous solution difficult to study. The approach is also time consuming and values can only be obtained at single points, making lubricant film thickness maps or profiles tedious to acquire.

Optical interferometric methods are well established and routinely used to obtain lubricant film thickness and profile shape data (11). The majority of optical interferometry work to date has studied 'hard' contacts between a metal or ceramic ball and a flat glass or sapphire disc. In the late 1960s Roberts and Tabor (8) showed that interferometry could also be used to produce reliable quantitative film thickness measurements from compliant, elastomeric contacts. The interference between a flat glass plate and a hemisphere or hemicylinder of smooth rubber was examined by reflected monochromatic light. It was found that conventional rubber surfaces were rough and poorly reflecting, so the interferometric observations were unsatisfactory (5). The addition of reflective coatings was not successful. A number of important developments took place in the early 1970s to improve image quality. First, Roberts *et al* (5) successfully developed optically smooth rubber samples, using hot compression moulding against polished glass or metal formers (7). Optically smooth rubber

surfaces with peak-to-valley surface roughness no greater than 20 nm (12) could be created using this process. Samples were developed further (6) by adding carbon black to the specimens before curing. This improved light absorption and therefore reduced light reflections not occurring at the contact surface, leading to improved image quality. Later, Roberts (5,7) introduced an Abbe prism to replace the flat glass disc. The illuminating beam was thus moved to a non-normal incidence to the contact area, so the amount of scattered light received by the detector was greatly reduced. This is shown schematically in Fig. 1. Using this method film thickness measurements down to ~ 10 nm where achieved.

The Abbe prism consists of a block of glass in the form of a right-angled prism with 30°-60°-90° triangular faces. A beam of light enters face AB, is refracted and undergoes total internal reflection from faces AC and BC, and enters the contact about three quarters of the way from A along the face AC. Here, a portion of the light is reflected from the glass surface while the remainder passes through any lubricant film to be reflected back from the ball surface. The two rays interfere at the reflecting surface AC and the resulting light is refracted on exiting face BC before being detected. To ensure total internal reflection occurs at faces AC and BC, an initial angle, α of 23° is calculated from Snell's law. From the design of an Abbe prism, this gives an exit angle equal to α. By rotating the prism and incident beam (in the plane of the diagram) around point A on the face AB, the interfering rays can be guided vertically upwards into the objective lens.

Early 'soft' contact work was restricted to static loading and studied fluid film flow squeezed from the contact zone over time (8,13,14). These initial investigations were

used to compare experimental results with existing theoretical models (15). A small, lateral, sinusoidal motion was introduced by Roberts (5,6) and visualisation of the contact was achieved with good image quality. Film thickness and friction results were taken at low sliding speeds in the range of 70 μm s^{-1} to 5 mm s^{-1}. More recently Kaneta *et al* (16,17) used a monochromatic optical interferometric technique to investigate the lubricant film thickness in a reciprocating, compliant, line contact. Investigations were made into the behaviour of o-ring seals by forming contacts between a nitrile rubber specimen of D-shaped cross section and a sinusoidally oscillating glass plate. Film thickness profiles were reported for a verity of positions within the stroke.

In the current study, Roberts' Abbe prism approach is developed further to study lubricant film thickness in unidirectional sliding, lubricated, compliant contact.

Apparatus

The experimental setup is shown in Fig. 2. The tribological contact consists of a rotating elastomer ball loaded against a transparent optical flat. The optical window is a BK7 glass prism (EdmundOptics, UK). This is naturally hydrophilic and was used without surface modification. The prism has a Young's Modulus, E, of 65 GPa, surface roughness, R_a of 9.4 nm, Poisson's ratio, v of 0.24 and refractive index, n, of 1.517. The prism is kept stationary while the ball rotates, so the system operates in pure sliding conditions. The elastomer ball has a radius of *ca* 11 mm, and is made of a thick PDMS layer on a smaller steel ball. The PDMS is supplied as a two part silicone elastomer kit, (Sylgard 184, Dow Corning, UK), and a base-to-curing agent mass ratio

of 10:1 was used for all elastomer samples. The PDMS is transparent; therefore reflections from within the specimen or the metallic sample mounting will interfere with the signal of interest. An opaque filler was added to the PDMS to reduce background scattering and absorb any non-reflected light. Only a small amount is required for this to be achieved and 0.5 wt % carbon black, CB, (Fluffy, Cabot, UK) was added to the uncured PDMS solution. The refractive index of the CB-filled PDMS was measured at 1.41 using an Abbe 60 refractometer (Bellingham and Stanley Ltd).

PDMS ball samples were created using a 'candle dipping' process, where uncured PDMS is layered onto a 19 mm diameter ASIS 440 bearing stainless steel ball until a layer *ca* 2 mm in thickness is created. Surface analysis of the CB-filled PDMS specimens was carried out using a Wyko NT9100 optical interferometer (Veeco, UK). Measurements were taken in the VSI mode and the camera was used with a X20 objective lens. Images were 640 x 450 pixels, which equates to a field of view of *ca* 575 x 430 μm. No filtering was used during measurements. A smooth surface finish of R_a = 70 ± 10 nm but with a large peak to valley height of 1 ± 0.2 μm was created using this moulding process. From dynamic mechanical analysis (DMA, Triton, UK), a Young's modulus of E = 2.8 MPa was measured for the CB-filled PDMS. A Poisson's ration of 0.49 was used when calculating the reduced elastic modulus.

The balls are mounted on a horizontal shaft within a small test fluid reservoir and loaded against the prism at the start of the test. DC servomotors, connected to a 100:1 reduction gear box, rotate the ball with accurate speed control to create entrainment

speed range of 1 μm s^{-1} to 3 mm s^{-1}. The normal load is applied as a dead weight *via* a lever arm and can be varied between 0.001 and 1 N.

Two test lubricants were used in the current study; a 95 % glycerol/water solution (GLY), η = 0.38 Pas and lab grade sunflower oil (SFO), η = 0.053 Pas, supplied by Unilever (Colworth). These were selected as they possess the same refractive index, n = 1.47, but differ in dynamic viscosity range by an order of magnitude. The refractive indices of both lubricants were measured, at atmospheric pressure, using an Abbe 60 refractometer. Under the test conditions used, the contact pressures were assumed to be low enough (less than 1 MPa) to have negligible effect on the refractive indices of the test lubricants. The calculated fringe visibility for both lubricants was 96 %.

Glycerol is hygroscopic and its viscosity varies very rapidly as small amounts of water are added (10), so its viscosity may change over time when it is exposed to air. To limit errors arising from this, for the current study a 5 wt.% solution water in glycerol was preferred to pure glycerol since its viscosity is far less sensitive to small changes in water content than pure glycerol.

All the lubricants studied were single phase and Newtonian over the range of shear rate from 1 to 1000 s^{-1}, which spans the test parameters. The viscosities of the test lubricants were measured using a Stabinger Viscometer (Anton Paar, UK) prior to testing. The test temperature was T = 22 ± 2 °C. The water used in the GLY solution was demineralised filtered water (Elga) while glycerol was supplied as 98 % pure grade (Sigma Aldrich, UK).

The test protocol was as follows. A new PDMS ball was used for each test and was cleaned by rinsing in distilled water and then a solution of sodium dodecylsulphonate in distilled water, followed by immersion in isopropanol in an ultrasonic bath for at least three minutes, and finally immersion in deionised water in an ultrasonic bath for at least 3 minutes. The glass prism was ultrasonically-cleaned in isopropanol, followed by acetone. The test rig was then assembled and ~ 60 ml lubricant added to partially submerge the ball. Load was then applied and interferomgrams taken at a series of entrainment speeds beginning from a low value and increasing stepwise.

Interference images

In order to measure film thickness, it is necessary to obtain interference fringes from a lubricated, PDMS on glass surface, as shown schematically in Fig. 3. The quality of the fringes and the accuracy of the measurements taken with the interferometer depend primarily on three conditions of the reflecting surfaces. The first is the surface finish. The intensity of a fringe will change from a maximum to a minimum (or *vice versa*) if the optical separation changes by $\frac{\lambda}{4n}$. It is therefore, important that the surfaces conform locally to a mean elevation which is less than $\frac{\lambda}{4n}$. Any deviation from the mean leads to a confusion of fringe order and hence a decrease in fringe visibility. To satisfy this, the surfaces must be optically smooth and both the glass and PDMS surfaces satisfy this criterion. The second condition concerns that of geometry. If meaningful measurements of elastic deformation are to be obtained, it is essential that the initial deviation from a perfect surface geometry is small in comparison with the deformation due to pressure. It is primarily for this reason that the experimentation

presented here is limited to a point contact. The third condition is that of reflectivity. For monochromatic interferometry, fringes of high visibility are obtained if the intensities of the two beams are equal ($I_1 = I_2$). Equal intensities can be achieved by controlling the reflectivity of the surfaces. It is important to note that high reflectivity is not a necessary requirement of two-beam interferometry. It is possible to obtain fringes of good visibility with very low reflectivity (and hence high absorption and/or transmission) provided that $I_1 \approx I_2$, although this is an inefficient use of the total light input. It is this feature of two-beam interferometry that makes film thickness measurements of surfaces with low reflectivity possible.

To obtain fringes of high visibility it is most important that the reflectivity of the optical window is comparable with that of the PDMS ball so as to make the intensities of the two interfering rays approximately equal ($I_1 \approx I_2$). For normal incidence, the reflectivity, R', between two non-magnetic materials follows the Fresnel equation;

$$R' = \left(\frac{n_1 - n_2}{n_1 + n_2} \right)^2 \qquad [7]$$

Once the intensities are known, the fringe visibility or clarity, V, is given as:

$$V = \frac{2\sqrt{I_1}\sqrt{I_2}}{I_1 + I_2}\gamma \qquad [8]$$

where n_1, n_2, I_1, I_2 and γ are the refractive indices of contacting media, interfering ray intensities and degree of coherence between the interference rays respectively. Figure

4 shows the fringe visibility for mutually-coherent interference rays over a range of lubricant refractive indices, for the tribological contact of interest. Predictably the visibility falls to zero at the refractive indices of the PDMS and BK7 glass. Maximum visibility is obtained at a mid point between the two media. Taking a minimum visibility value of 70 %, a number of lubricant refractive index ranges are available, *i.e.* n = 1 to 1.35, 1.44 to 1.49 and 1.59 upwards. By varying the refractive index of the glass prism it becomes possible to investigate lubricants whose refractive index lie outside these ranges.

A 20 W LED light source (TruOpto) was used for illumination, which is monochromatic with wavelength λ = 625 to 635 nm. The absolute thickness of lubricant film was found by counting fringes generated at the rear of contact as the entrainment speed is increased and the surfaces separate (5). Due to the poor reflectivity of the contacting surfaces, an image intensifying camera was needed to capture the interferograms.

A series of, cropped, typical low-speed interferograms obtained in this study are shown in Fig. 5(a), (b), (c), and (d). These were taken at u = 0.02, 0.25, 0.33, 1.31 mm s^{-1} respectively, all at an applied load = 3 mN and with GLY as lubricant. Lubricant flows along the X plane from left to right. Interferograms were captured as 512x512 pixel arrays, with a calibrated pixel size of 3.2 μm. The calculated Hertzian contact radius was *ca* 0.18 mm for all images in Fig. 5. The monochromatic system shows good detail in film shape and it can be seen that for all the images, the minimum film thickness occurs at the lubricant outlet constriction.

Film thickness maps were extracted from Figs. 5(a) to (d) by image analysis and are shown in Figs. 6(a) to (d). A full X-Y coordinate map of the fringe positions, number and intensity is built up for each image. To do this, columns with less than one full fringe and all intensity data outside the first and last fringes detected are filtered out. The minimum fringe number/position and film thickness value is inputted from which all film thickness values are then calculated. The minimum film thickness fringe was used as the datum point due to the certainty in its location. The minimum film thickness value was obtained by counting fringe changes at the rear of the contact from zero entrainment speed upward. For film thickness values between maxima and minima values, the grey scale intensity was used to interpolate between points, giving a clear indication of film thickness gradient. This was similar to the procedure used by Roberts *et al* (5). By including all grey scale data, the correct shape of the contact could be obtained, in particular the shape and extent of the outlet constriction. Another benefit of this technique is that surface roughness can also be plotted. The system can only count upward changes in phase, therefore to avoid confusion between phase changes due to asperities, areas of the image can be selected that are to be ignored during fringe mapping. This allows asperities to be filtered out and then re-inserted during interpolation of grey scale data. Before a final film thickness map of the contact area is produced, any spurious fringes which have formed as a result of asperities or dirt/interference detected beyond the main contact region, are removed. Any columns, within the contact area where no fringes are detected are assumed to be the average of their immediate neighbours.

For each case in Figs. 5 and 6, the minimum film thickness occurs directly behind the centre of the contact. At low values of u, two regions of minimum film thickness

occur, close to the centre line and at the sides. Although this is not clearly shown in the film thickness maps because of the coarseness of the grey scale analysis, it is suggested in the interferograms. These side lobes have been predicted numerically by Hamrock and Dowson (4) and demonstrated experimentally by Roberts *et al* (5).

Results

Effect of load

Film thickness profiles along the X axis for Y = 0, were obtained by the same method as that used to create film thickness maps discussed above. Profiles of the tribological contact lubricated with GLY at similar entrainment speeds, for three different applied loads, are presented in Figs. 7(a), (b) and (c). The minimum film thickness position was used as a universal reference point to compare the plots. The central contact point was not used as no geometry reference system was available during experimental testing. This is the case for all subsequent figures. The profiles show details of film shape and, in particular, the minimum film thickness located in the outlet region. Surface topography and asperities are also visible due to interpolation of gray scale intensity between fringes.

GLY profiles show some variation in contact size; this is most notable at 50 mN load, Fig. 7(c). In profiles at u = 0.2 and 0.61 mm s^{-1}, the contact size appears to vary by about *ca* 100 µm. This suggests a possible error in load of 1 to 2 mN may be occurring. The contact size at 3 mN load, shown in Fig. 7(a), appears to vary by *ca* 40 µm, while at 35 mN load, contact size variation appears to be negligible. This may be

a result of vibrations in the test apparatus, and illustrates the sensitivity of I-EHL lubricant films to load.

As load is increased, noise in the profile plots also increases. The larger contact size increases the likelihood of asperities being present. Asperities do appear to be present in a number of the profiles, most notably for profiles at low film thickness values; however this would not cause noise along the entire profile. At higher loads, surface roughness effects may be more visible due to the lower film thickness values. Film thickness values are below the peak to valley height of 1 ± 0.2 μm, however h is still above the roughness, R_a.

Figure 8 compares film thickness and pressure profiles, along Y = 0, for the tribological contact lubricated with GLY under 3 and 50 mN applied load. Film thickness profiles were taken from Fig. 7(a) and (c) at similar entrainment speeds of 0.65 and 0.61 mms^{-1}, respectively. To accurately calculate the pressure, the film thickness profiles obtained from interferometric measurement, were extended to five times the Hertzian radius on the inlet side. This was achieved by assuming the contact profile deviates back to the radius of curvature of the ball at radii outside the measured interferometric profiles. The pressure profiles were calculated by an inverse method based on inputting the experimentally-measured film thicknesses to a numerical Reynolds equation solver as described by Cameron (18). The solver discretised the domain using finite differences and any pressures below the gauge pressure were set to the gauge pressure. Film profiles at the same applied load show similar areas under the pressure curves, as expected.

In Fig. 8, it can be seen that the maximum pressure occurs just behind the centre of the contact for the low load case. However for the high load case, the maximum pressure occurs closer the Hertzian centre. This was predicted by Hamrock and Dowson (4). For an order of magnitude change in the applied load there is a considerable change in the pressure profile of *ca* 6 times p_{max}. However there is a less significant change in the film thickness profile, only a change of *ca* 2.5 *h*.

Figure 9(a) and (b) show the central and minimum film thickness values, respectively, for applied loads of 3, 35 and 50 mN for the tribological contact lubricated with GLY. Theoretical predictions from equations (3) and (4) are also shown as solid or dashed lines. In hard, metallic contacts the central film thickness, h_c is normally positioned on the flat plateau region bounded by the horseshoe shaped constriction, making it a significant value as it describes a large proportion of the contact. For compliant contacts h_c is less significant, due to the exit constriction being restricted to the rear of the contact, i.e. not developing side lobes. It is also observed that the majority of the contacts in Fig. 7 form a hydrodynamic wedge. Therefore position of the h_c, was defined as the middle of the detected profile.

It is observed that the predicted film thickness values are some what greater than the experimental results. Equations [3] and [4], solved by Dowson and Hamrock (4), where fitted to a small range of values of $U = 5\text{x } 10^{-9}$ to $5 \text{ x } 10^{-8}$ and $W = 0.2$ to $2 \text{ x } 10^{-3}$. These are somewhat larger than the experimental measurements performed in this study, over a range of values of $U = 9\text{x } 10^{-12}$ to $5 \text{ x } 10^{-9}$ and $W = 3 \text{ x } 10^{-6}$ to $5 \text{ x } 10^{-5}$. This may account for the large disagreement between experimental and theoretical plots.

Influence of entrainment speed

Figure 10 shows central film thickness profiles at various entrainment speeds for SFO under 3 mN applied load. Profiles are taken in the direction of flow, along the X axis.

Compared to GLY there appears to be greater noise in the SFO plots. The test sample used may have been of a larger surface roughness. This is unlikely, however, as noise is not present in results from Fig. 7 at similar values of h for GLY. Since SFO and GLY were used as supplied, they may not necessarily be free of surface-active components or debris, which could build up within the contact area during testing and interfere with imaging. SFO is a natural product containing impurities, among which are surface active free fatty acids. This may have caused the difference in noise between the two test lubricants. Another possible reason for the difference in noise between images is errors/differences in focus.

Lubricant film thickness profiles for SFO at u = 0.66 and 0.21 mm s^{-1}, shown in Fig 10, were used to calculate pressure profiles. The resultant pressure profiles along the centre line in the sliding direction are shown in Fig. 11. The pressure in the inlet region is greater for u = 0.66 mm s^{-1}. However, inside the contact, the values for the pressure are higher for the low speed case, u = 0.21 mm s^{-1}. As the entrainment speed and consequently the film thickness is reduced, the pressure approaches closer to the Hertzian profile. However even at the lower speed there is still a significant rise in pressure in the inlet region and the pressure profile remains skewed towards the exit region.

Effect of viscosity

Figure 12 compares film thickness profiles and calculated pressure profiles for SFO and GLY, along Y = 0, at 3 mN applied load. Profiles were taken from Fig. 7(a) and Fig. 8 at similar entrainment speeds of 0.65 and 0.66 mm s^{-1}, respectively. For the high viscosity case, GLY, the maximum pressure occurs near the Hertzian contact centre. The curved or near-hemispherical nature of the pressure plot is indicative of the wedge-shaped film thickness profile. However, for the low viscosity case, SFO, the maximum pressure occurs just before the contact exit region due to the formation of the pressure constriction. For a one order of magnitude change in the viscosity there is a doubling of the pressure and the film thickness. This approximate direct proportionality between η and h is not surprising as the pressures within the contact, operating under I-EHL conditions, are not great enough to change the lubricant viscosity.

The pressure spikes found when dealing with materials of high elastic modulus (19) are not evident in these results for a low elastic modulus body in contact. The lack of a pressure spike is probably due to the lack of piezo-viscous effects of the fluid in the contact for compliant materials. This is in turn due to the fact that considerably less pressure is generated in a compliant contact than in a contact with high elastic modulus materials. This was predicted by Hamrock and Dowson (4).

Figure 13 compares experimental central and minimum film thickness data for both test lubricants over the entrainment speed range. Similar to Fig. 9 the theoretical

values are observed to be much larger than the experimental results. By varying the power law coefficients, the following best-fits were obtained for all experimental conditions;

$$h_c = 3.3U^{0.63}W^{-0.13}R \qquad [9]$$

$$h_m = 2.8U^{0.68}W^{-0.20}R \qquad [10]$$

Equations [9] and [10] both show different dependences on the speed and load parameters from equations [3] and [4] which were derived from simulations of compliant contacts. It should be noted that a small change in the power law coefficients will produce a large change in film thickness values.

Theoretical profile shape

A full numerical solution for compliant EHL given by de Vicente *et al* (2), was used for comparison with measured film thickness profiles. The solution approach was a standard finite difference one with a 256x128 grid and Reynolds cavitation boundary conditions. Figure 14.a) shows the predicted film thickness obtained using de Vicente's model for the tribological contact of interest lubricated with SFO, at Q = 3 mN and u = 0.66 mm s^{-1}. Compared to conventional EHL contacts the 'horse shoe' outlet constriction, a characteristic of EHL contacts, is restricted to the exit, instead of extending towards the inlet region. In this I-EHL contact (Fig 14.a) it can be observed that the film has a noticeable gradient within the Hertzian contact region, compared to conventional hard EHL contacts. In this way the film takes on a

'convergent wedge' shape similar to that used in many hydrodynamic bearings. It is likely that this 'wedge' is largely responsible for generating fluid pressure and therefore the load-carrying capacity of the contact.

Figure 14.b) shows the corresponding experimental film thickness map for the tribological contact of interest lubricated with SFO, at Q = 3 mN and u = 0.66 mm s^{-1}. It should be noted that the experimental result is symmetrical through Y = 0. This is because only one half of the interference image was used in this case due to poor fringe quality in the left hand side. It can be seen that there is reasonable qualitative agreement with the theoretical results predicted by de Vicente's model. The experimental results show both a reduced horseshoe, which is limited to the rear of the contact, and 'wedge' shaped film thickness profile within the Hertzian contact region. However, it can be observed that quantitative agreement between absolute film thickness values is not achieved; the experiments showing a generally thinner lubricant film. This comparison is clearly shown in Fig. 15 where the central film thickness profiles are plotted. Across the main contact region the theoretical film thickness values are *ca* 0.075 μm greater than those experimentally measured. However, a larger difference, *ca* 0.2 μm, in the predicted and experimental minimum film thickness is observed. It would be expected that such differences in film thickness profiles, particularly the increased exit constriction of the experimentally measured profile, would lead to a skew in the pressure profile towards the outlet region. This, allied with the overall lower absolute film thickness, suggests higher local film pressures, all else being equal. But further comparison of the film thickness maps shows that the horseshoe present in the experimental result does not extend as

far towards the bearing inlet. This would be likely lead to increased side leakage and require the film to adopt a more 'convergent shape'.

One possible cause for the discrepancy between De Vicente's model and the experimental result is that the model assumes the contact comprises of a glass flat and PDMS ball. However, in this work, the ball is made of a stainless PDMS layer on a steel substrate. The problem of elastic contact between non-conforming coated surfaces has received much attention over the years. It is important in such contacts to correct for the effect of the substrate; a new effective elastic modulus and thus contact size should be calculated. The elastic mismatch between the coating and the substrate can be characterised by the Dundurs' parameters (22,23). For the tribological contact of interest in the current study, the Dundurs' parameter values lie outside the limits set out by ref (22). This is, in part, due to the large difference between elastic moduli of the contacting surfaces and the large coating thickness compared to the Hertzian contact size. However, Oliveria and Bower were investigating 'hard' coatings in line contacts, unlike the compliant coating in the current study. Meijers (24) and Liu *et al* (25) give solutions for incompressible materials with Poissons ratio up to 0.5, in line and point contacts respectively. Both show that if the coating thickness is large compared to the Hertzian contact radius, for $\nu = 0.5$; the substrate has negligible effect on the contact size.

However, the behaviour of the contacting surfaces will also depend on the nature of the attachment of the PDMS coating to the steel substrate (20). There are various possibilities: the layer may maintain contact with the substrate at all points, but be free to slip without frictional restraint. This seems unlikely due to the low load, low

pressure and slow entrainment conditions. On the other hand the layer may be bonded on to the substrate and thus slip may occur when the shear traction at the interface exceeds a limiting shear stress; or the layer, initially in complete contact with the substrate, may partially lift from the substrate under load. The latter seems plausible as PDMS is known to sweat un-cured monomer (21). This would allow for the steel PDMS interface to be lubricated over time, gradually separating the surfaces and breaking the adhesive bond between PDMS and steel.

Concluding remarks

It has been shown that monochromatic optical interferometry can be used to measure lubricant film thickness in a compliant contact under low load conditions across a low entrainment speed range. Film thickness data from the contact correlated reasonably well with numerical film thickness predictions. Film thickness values were obtained from nano to the micron scale.

New fits for the Hamrock and Dowson lubricant film thickness equations for an I-EHL contact for materials of low elastic modulus (4) were obtained. These showed slight differences in dependence on the dimensionless speed and load parameters from those already available in the literature. It was shown that the experimental film profiles vary markedly with both U and W and at higher u a sharp constriction appears at the outlet and the centre of pressure moves towards the rear of the bearing. The outlet of the bearing is therefore responsible for a larger component of the total load support. This is in contrast to film shapes previously predicted by various numerical methods available in the literature. Further experimental investigation is required

using a solid PDMS ball to establish the whether these discrepancies result from the use of a layered PDMS on steel substrate ball in the current study. This will establish whether or not the unconventional film profiles observed in the current study are a genuine feature of I-EHL contacts.

The ability to create film thickness maps using the optical interferometric technique has also been shown. These maps are relatively easy to acquire and not time-consuming. It is not yet possible, however, to generate maps across the entire contact area, in particular obtaining the correct shape of the side lobes is not yet achievable.

References

(1) Poll, G. and Gabelli, A. (1992), "Formation of lubricant film in rotary sealing contacts: Part II - A new measuring principle for lubricant film thickness", Journal of Tribology, Transactions of the ASME 114, 290-296.

(2) De Vicente J. Stokes J. R. and Spikes. H. A, (2005), "The frictional properties of Newtonian fluids in rolling-sliding soft-EHL contact", Tribology Letters. 20, 3-4, pp. 273-286.

(3) Esfahanian M. and Hamrock. B. J, (1991). "Fluid-film lubrication regimes revisited", Tribology Transactions. 34, pp. 628-632.

(4) Hamrock. B. J. and Dowson. D, (1977). "Elastrohydrodynamic lubrication of elliptical contacts for materials of low elastic modulus 1 - Fully flooded conjunction". NASA TN D-8528 .

(5) Roberts. A. D. and Tabor. D, (1971). "The extrusion of liquids between highly elastic solids". Proc. R. Soc. Lond. A. 325, pp.323-345.

(6) Roberts A. D, (1971). "The shear of thin liquid films". Journal of Physics D. 4, 3, pp. 433-440.

(7) Richards. S. C. and Roberts. A. D, (1992). "Boundary lubrication of rubber by aqueous surfactant". Phys. D: Appl. Phys. 25, pp. A76-A80.

(8) Roberts A. D. and Tabor. D, (1968). "Fluid film lubrication of rubber - an interferometric study". Wear. 2, pp. 163-166.

(9) Poll. G, Gabelli. A, Binnington. P, and Qu. J (1992). "Dynamic mapping of rotary lip seal lubricant films by fluorescent image processing". Proceedings of the 13th Annual Conference on Fluid Sealing, BHRA. pp. 55-57.

(10) Bongaerts. J. H. H, Day. J. P. R, Marriott. C, Pudney. P. D. A, and Williamson. A M, (2008). "In situ confocal Raman spectroscopy of lubricants in a soft elastohydrodynamic tribological contact". Journal of Applied Physics. 104. DOI:10.1063/1.2952054.

(11) Spikes. H. A, (1999). "Thin films in elastohydrodynamic lubrication; the contribution of experiment". Proc. Instn. Mech. Engrs. 213, J, pp. 335-352

(12) Roberts. A. D, (1976). "Optical rubber". Rubber developments. 29, 1, pp. 7-11.

(13) Roberts. A. D, (1971). "Squeeze films between rubber and glass". Journal of Physics D. 4, 3, pp. 423-432.

(14) Field. G. J, and Nau. B. S, (1975). "Lubrication behaviour in loaded rubber contacts". Wear. 65, pp. 79-85.

(15) McClune. C. R, and Briscoe. B. J, (1977). "Elastohydrodynamic films formed between a rubber cylinder and glass plate: a comparison of theory and experiment". Journal of Physics D: Applied Physics.10, pp. 587-596.

(16) Kaneta. M, Todoroki. H, and Nishikawa. H, (2000). "Tribology of flexible seals for reciprocating motion". Journal of Tribology. 122, pp. 787-795.

(17) Kaneta. M, Takeshima. T, Togami. S, and Nishikawa. H, (2005). "Stribeck curve in reciprocating seals". 18th International Conference on Fluid Sealing, Antwerp, BHRG. pp. 333-347.

(18) Cameron. A, (1971). "Basic Lubrication Theory". Longman. London, UK.

(19) Hamrock. B. J, and Dowson. D, (1977). "Isothermal Elastohydrodynamic Lubrication of Point Contacts. Part III-Fully Flooded Results". J.Lubr.Technol. 99, 2, pp. 264-276.

(20) Johnson. K. L, (2003). "Contact Mechanics". Cambridge University Press.

(21) Hillborg. H, and Gedde. U. W, (1998). "Hydrophobicity recovery of polydimethylsiloxane after exposure to corona discharges". Polymer. 39, 10, pp.

1991-1998.

(22) Oliveira. S. A. G, and Bower. A. F, (1996). "An analysis of fracture and delamination in thin coatings subjected to contact loading". Wear. 198, pp. 15-32.

(23) Olver. A. V, (1997). "Correlation factors for the 2D coated Hertzian contact problem". Wear. 212, pp. 265-267.

(24) Meijers. P, (1968). "The contact problem of a rigid cylinder on an elastic layer". Appl.Sci.Res. 18, pp. 353-383.

(25) Liu. S.B, Peyronnel. A, Wang. Q. J, and Keer. L. M, (2005). "An extension of the Hertz theory for three-dimensional coated bodies". Tribology Letters. 18, 3, pp. 303-314.

Figure 1. Tribological contact of interest

Figure 2. Schematic of the optical setup and tribological contact (not to scale). Left: side view; right: front view along the axis of rotation of the ball. The black double-headed arrows indicate the image axes.

Figure 3. Two beam interferometry system.

Figure 4. Fringe visibility versus lubricant refractive index calculated from equation [8].

Figure 5. Interferograms of the tribological contact under 3 mN applied load, lubricated with GLY. At u = 0.02, 0.25, 0.33 and 1.31 mm s^{-1} for images (a), (b). (c) and (d) respectively. Lubricant flows from left to right, in the X direction.

Figure 6. Film thickness maps of the tribological contact under 3 mN applied load, lubricated with GLY. At u = 0.02, 0.25, 0.33 and 1.31 mm s^{-1} for images (a), (b). (c) and (d) respectively. Lubricant flows from left to right, in the X direction. Film thickness is expressed as RGB intensity, values indicated in the colour bar to the right of the figure.

Figure 7. Film thickness profiles for GLY at applied loads of (a) 3, (b) 35 and (c) 50 mN.

Figure 8. Film thickness (solid lines) and pressure (dashed) profiles for Q = 3 mN and 50 mN, at u = 0.65 and 0.61 mm s^{-1} respectively, for tribological contacts lubricated with GLY.

Figure 9. Measured (a) central film thickness and (b) minimum film thickness values at Q = 3, 35 and 50 mN for the tribological contact lubricated with GLY, across the entrainment speed range of 0 – 1.8 mm s^{-1}. Theoretical predictions from equations [3] and [4] are also shown as solid or dashed lines.

Figure 10. Film thickness profiles of the tribological contact lubricated with SFO, under 3 mN applied load at u = 0.016, 0.21, 0.66, 1.33 mm s^{-1}.

Figure 11. Film thickness (solid lines) and pressure (dashed) profiles for u = 0.66 (red) and 0.21 (black) mm s^{-1}, under 3 mN load.

Figure 12. Film thickness (solid lines) and pressure (dashed) profiles for GLY (red) and SFO (black) under 3 mN applied load at *ca* u = 0.66 mm s^{-1}.

Figure 13. Measured central (solid) and minimum (open) film thickness values for GLY (squares), and SFO (circles) for the tribological contact under 3 mN applied load. Numerical predictions for central and minimum film thickness values are plotted as solid and dashed lines respectively.

Figure 14. Film thickness maps of the tribological contact of interest under 3 mN of load and at u = 0.66 mm s^{-1}. a) De Vicente *et al.* model (2). b) Experimental result.

Film thickness is expressed as RGB intensity, values indicated in the colour bar to the right of the figure.

Figure 15. Measured film thickness profile (solid) and predicted film thickness profile (dashed) from De Vicente *et al.* (2), for the tribological contact of interest lubricated with SFO, at Q = 3 mN and u = 0.66 mm s^{-1}.

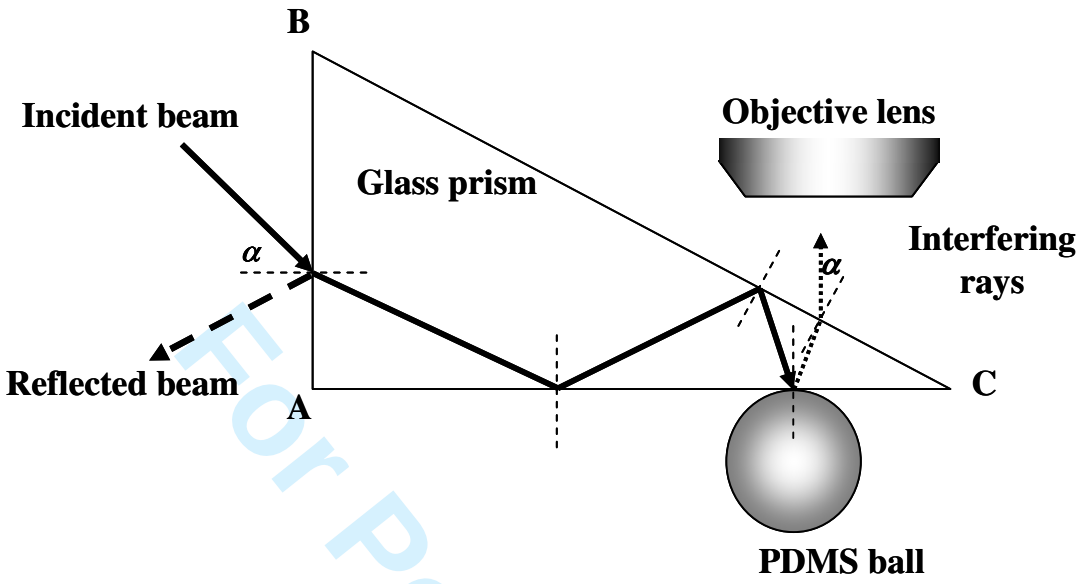

Figure 1.

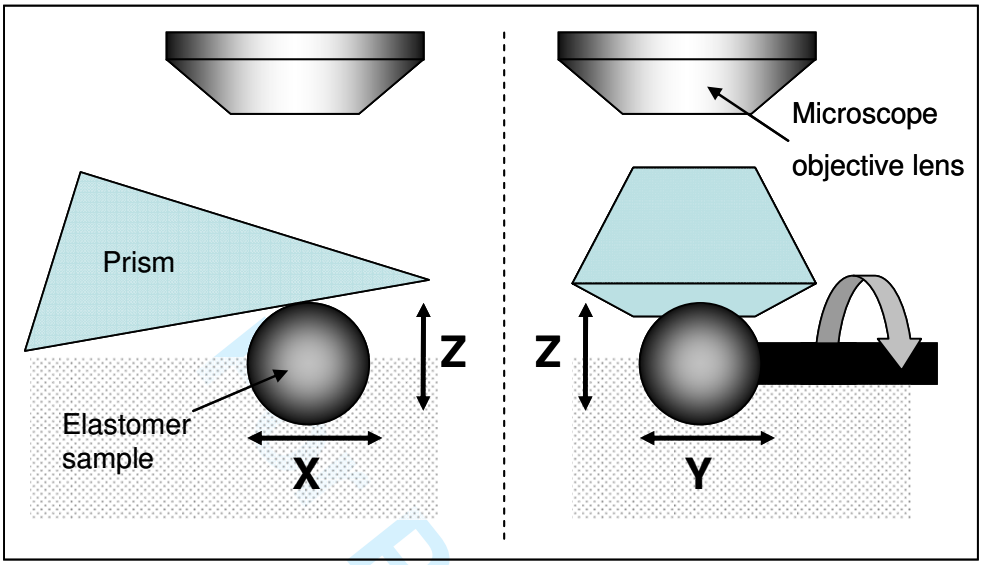

Figure 2.

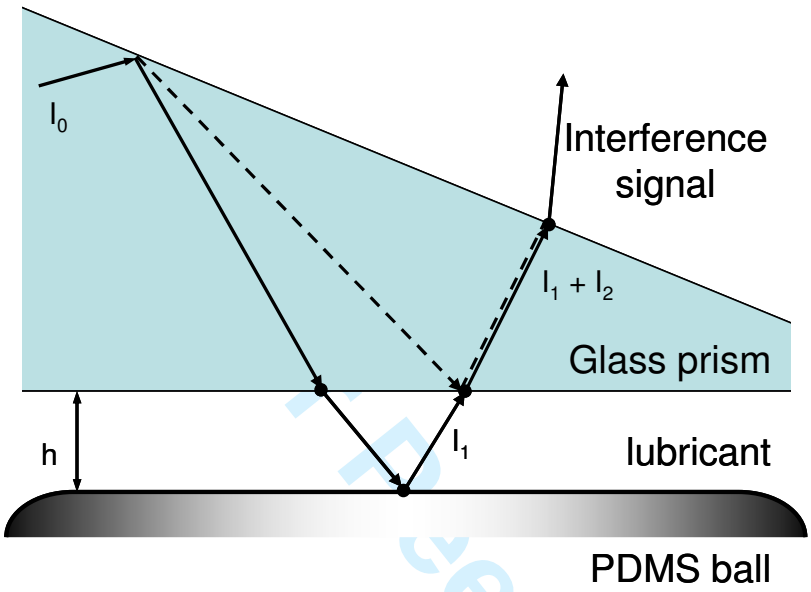

Figure 3.

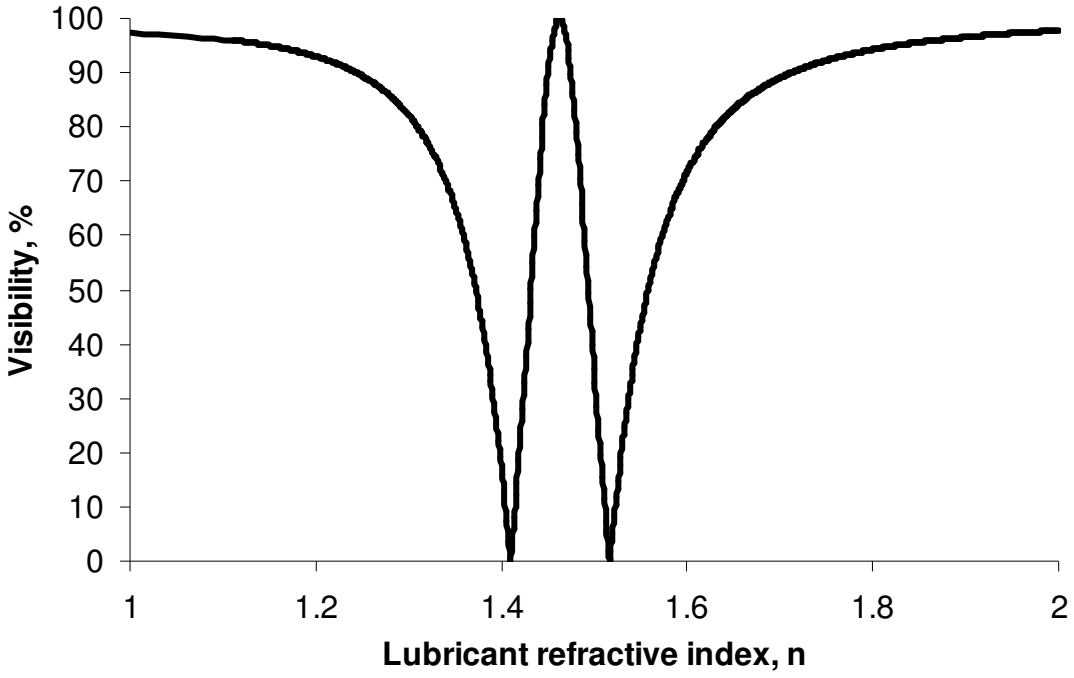

Figure 4.

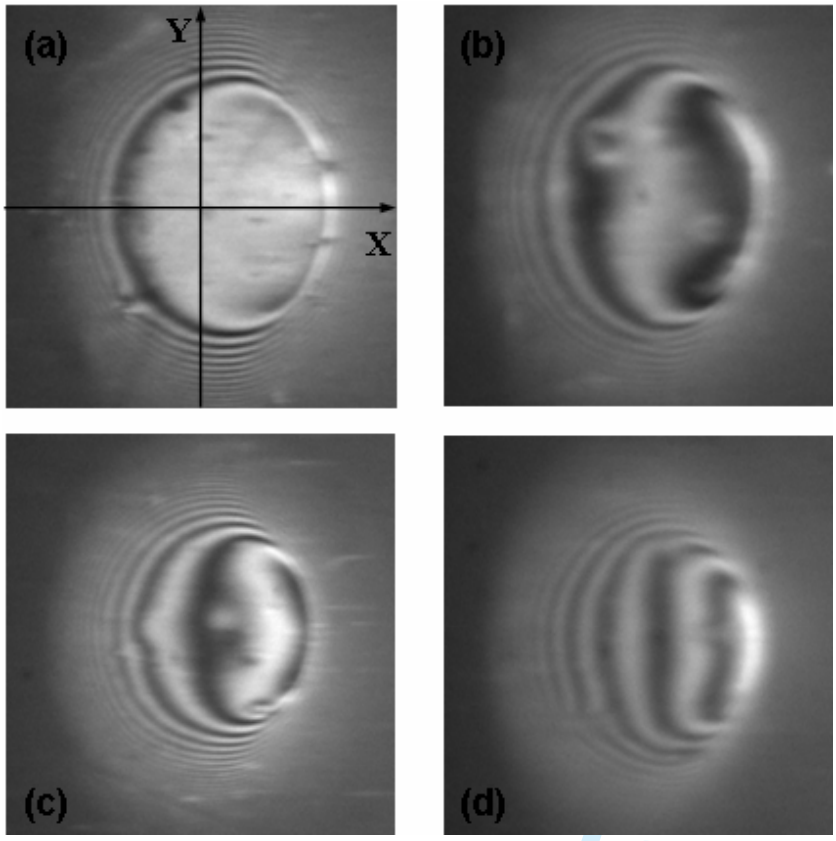

Figure 5.

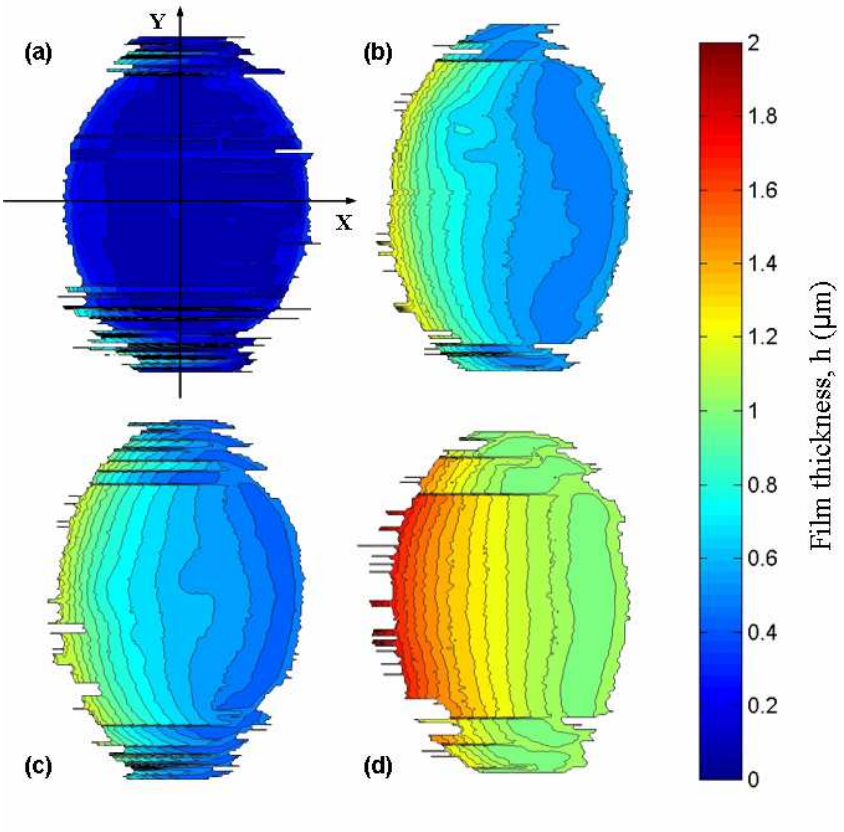

Figure 6.

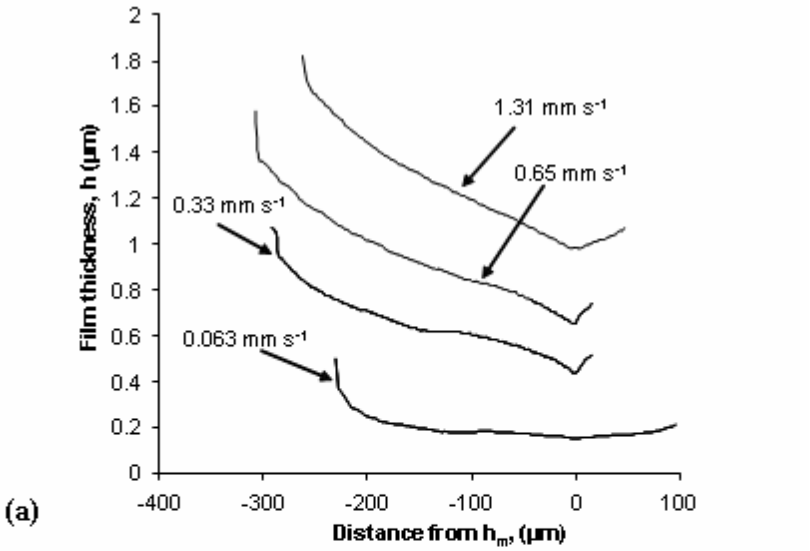
Film thickness, h (μm)
Distance from h_m, (μm)
1.31 mm s-1
0.65 mm s-1
0.33 mm s-1
0.063 mm s-1

(a)

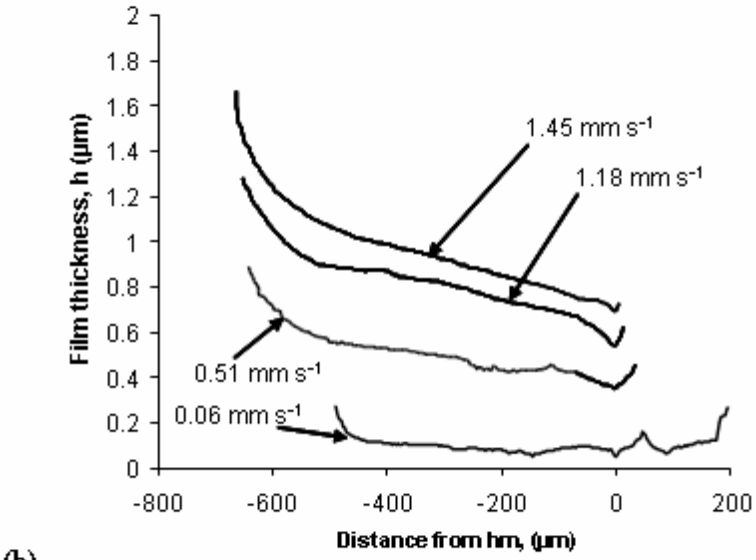
Film thickness, h (μm)
Distance from hm, (μm)
1.45 mm s-1
1.18 mm s-1
0.51 mm s-1
0.06 mm s-1

(b)

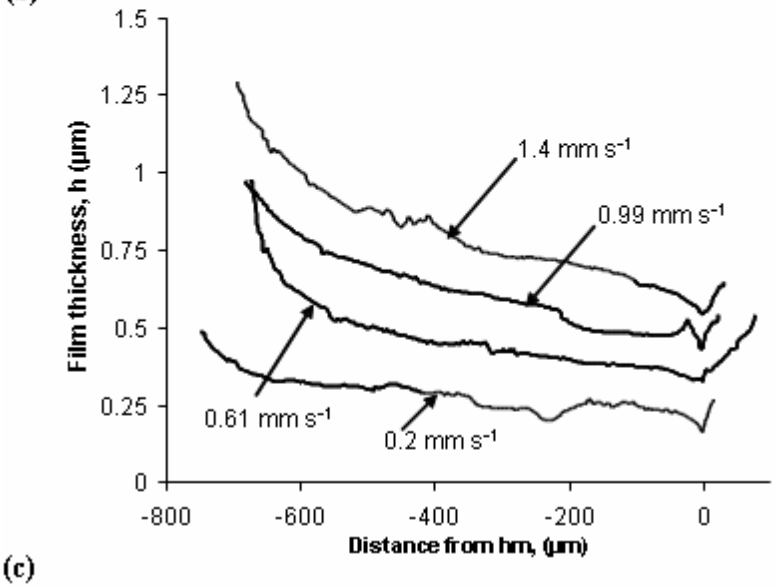
Film thickness, h (μm)
Distance from hm, (μm)
1.4 mm s-1
0.99 mm s-1
0.61 mm s-1
0.2 mm s-1

(c)

Figure 7.

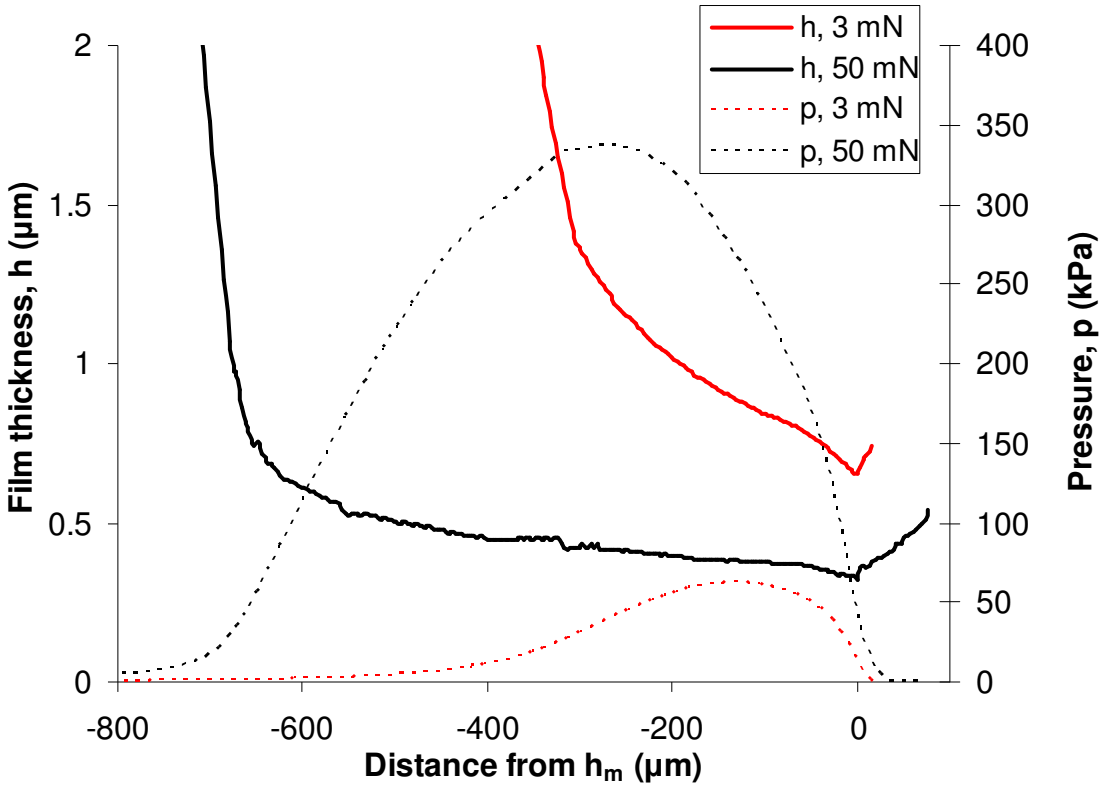

Figure 8.

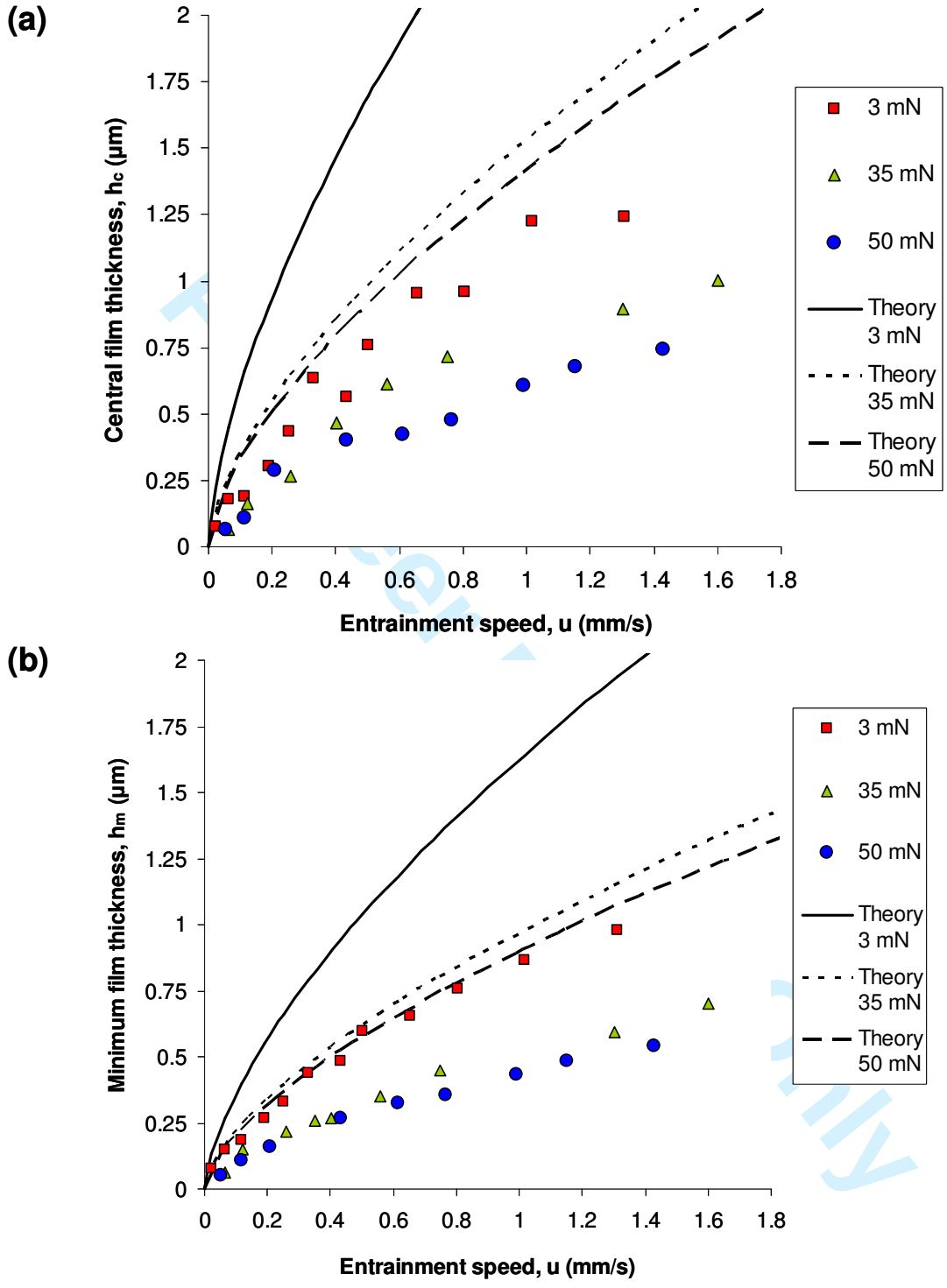

Figure 9.

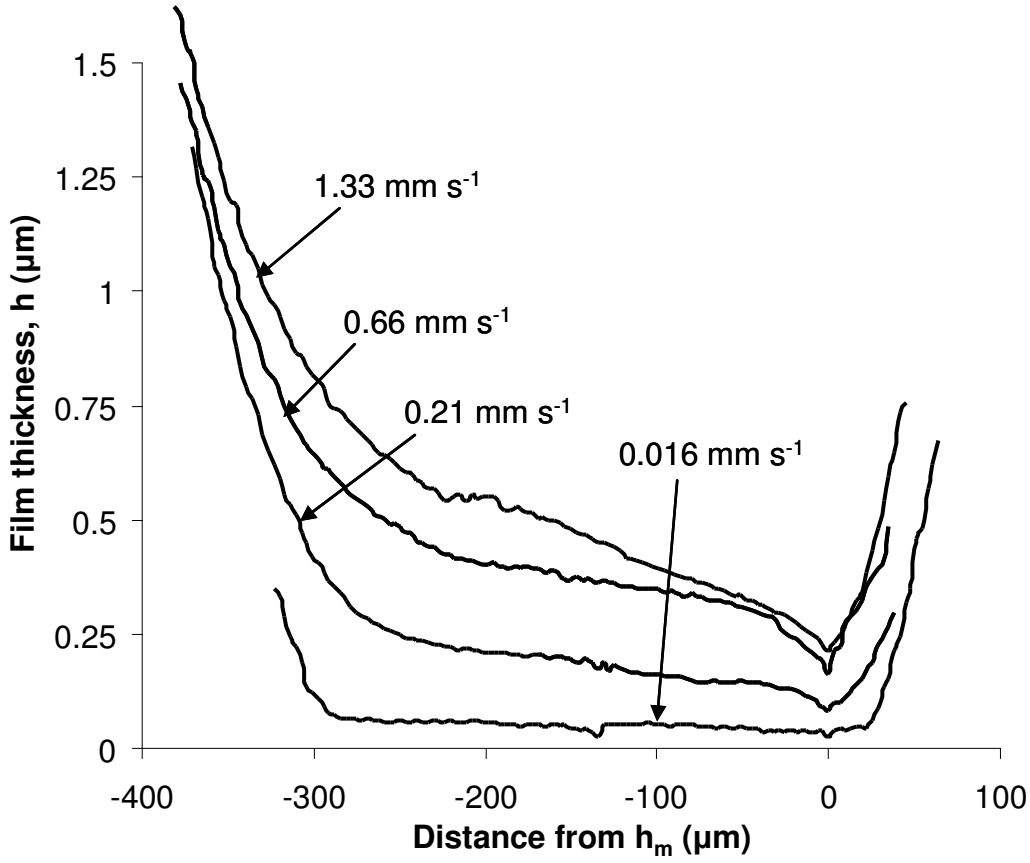

Figure 10.

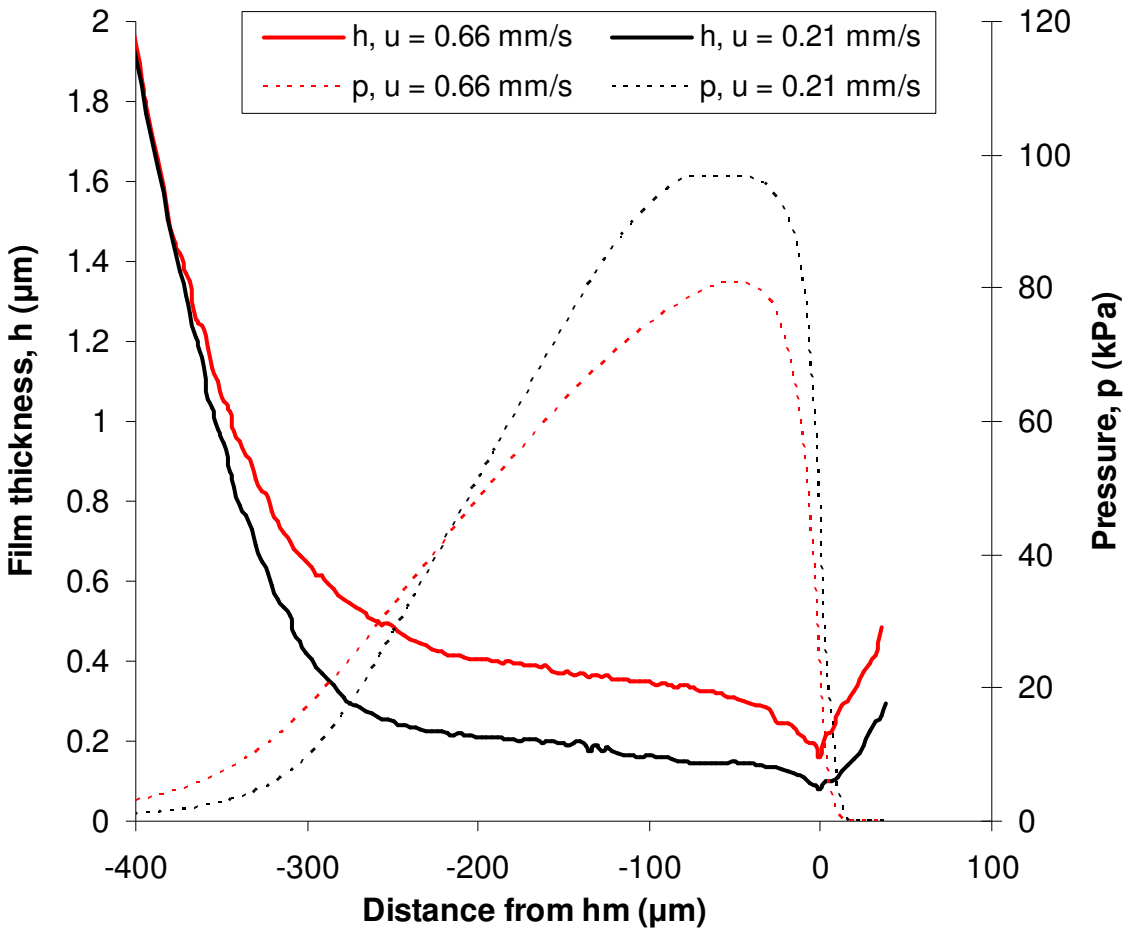

Figure 11.

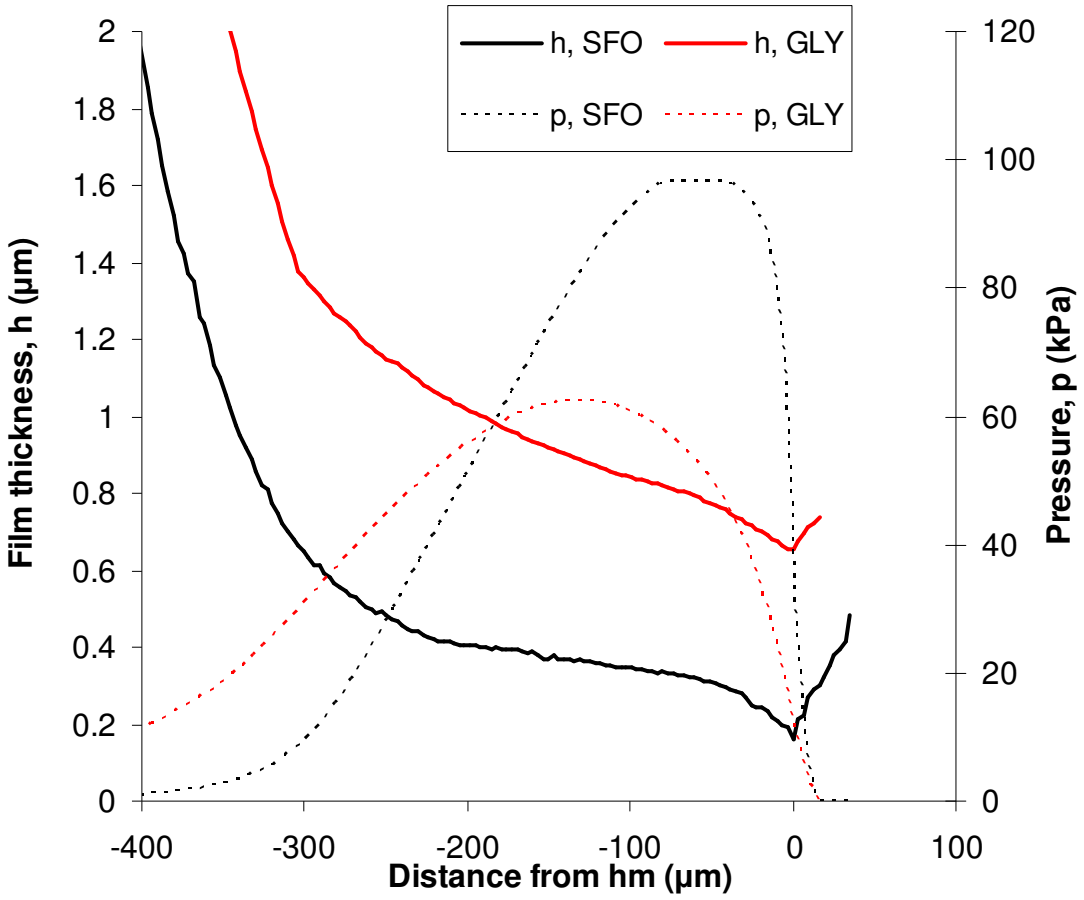

Figure 12.

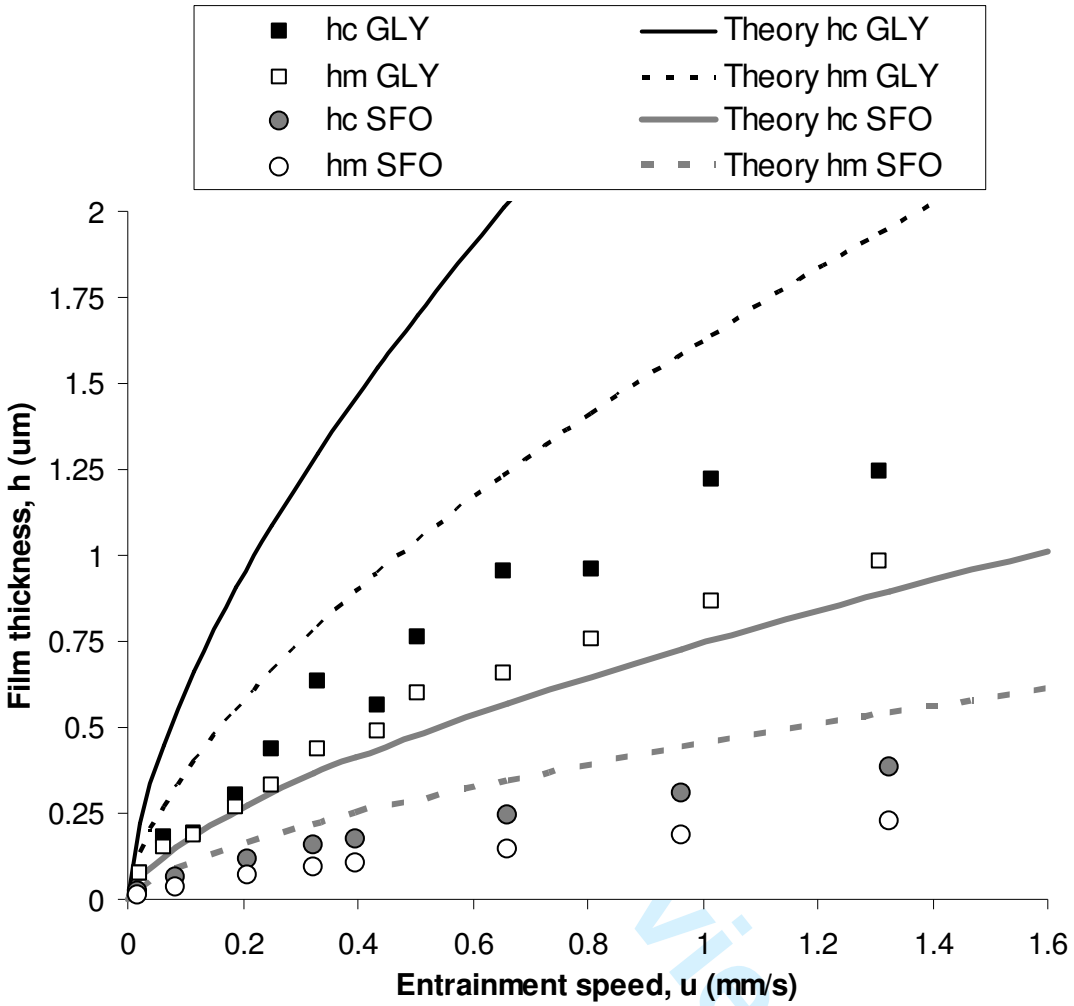

Figure 13.

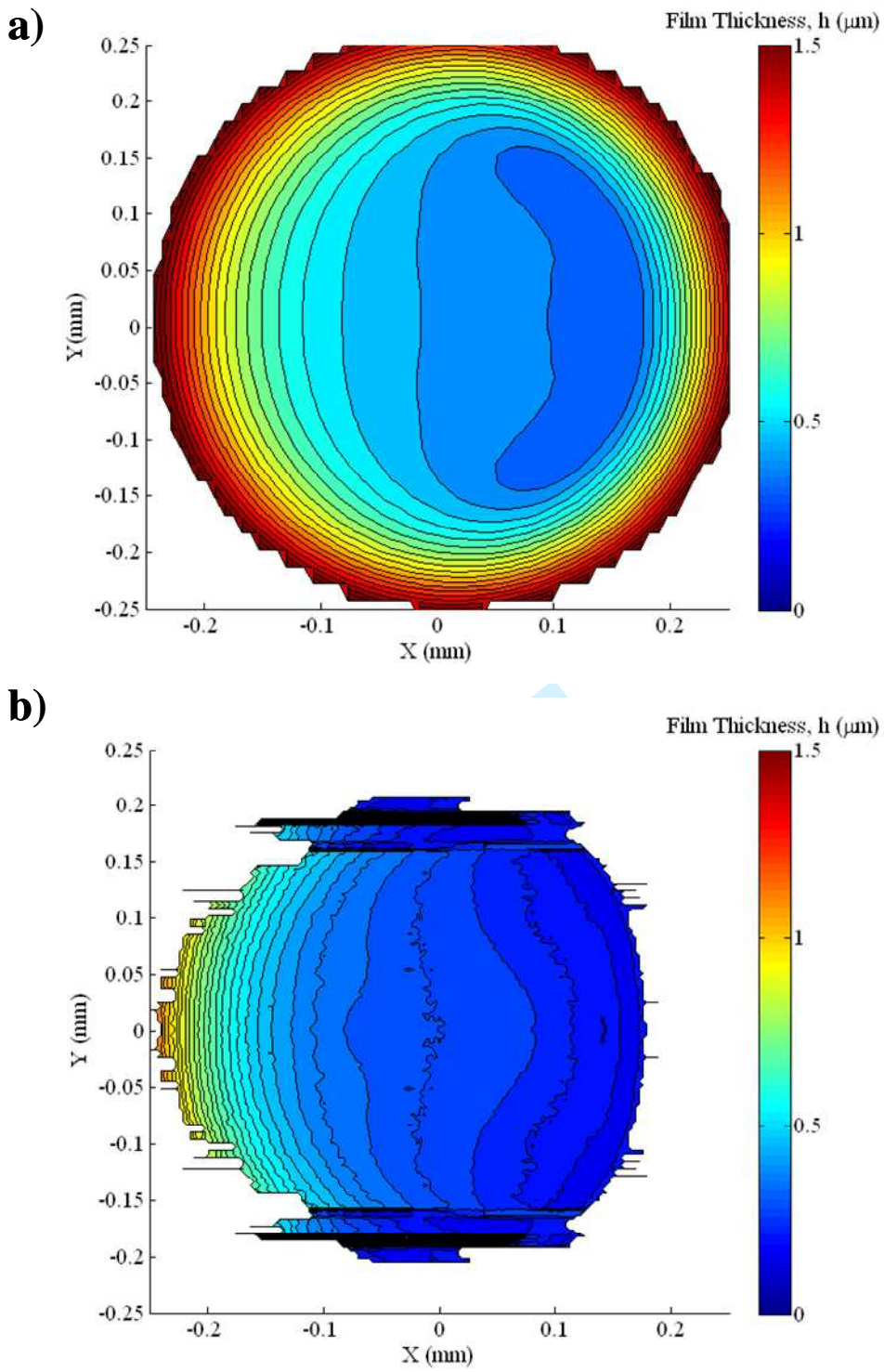

Figure 14.

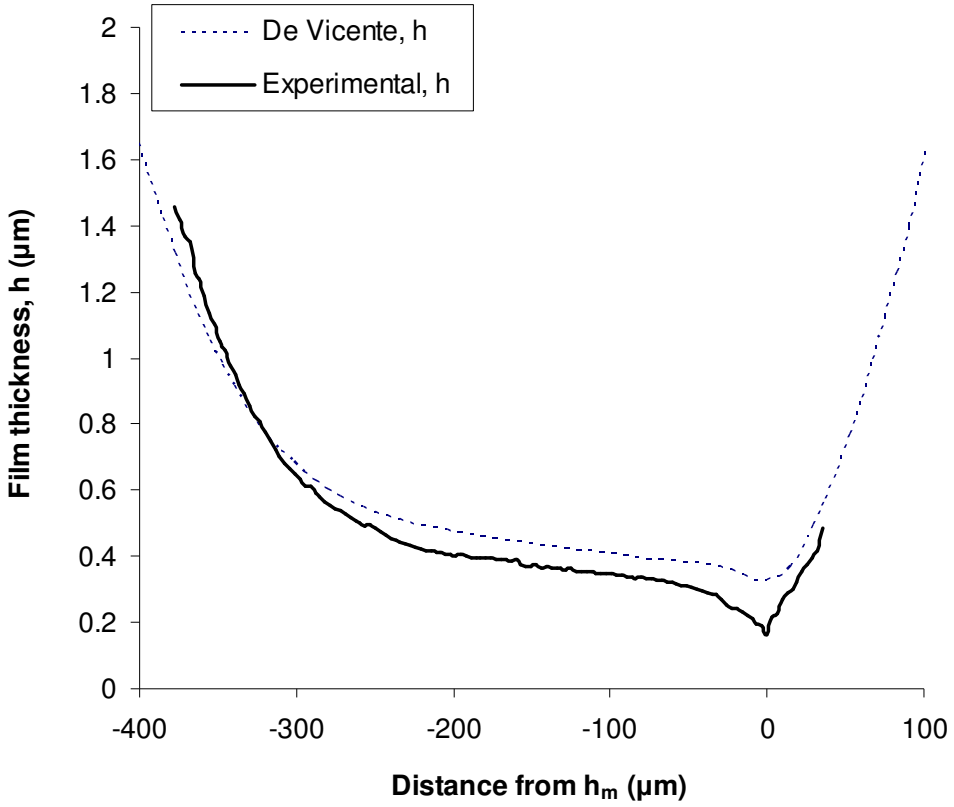

Figure 15.